Contents lists available at ScienceDirect

Electrochimica Acta

Research Paper

Improve the catalytic property of $La_{0.6}Sr_{0.4}Co_{0.2}Fe_{0.8}O_3/Ce_{0.9}Gd_{0.1}O_2$ (LSCF/CGO) cathodes with CuO nanoparticles infiltration

Chenlong Gao[a,1], Yingjun Liu[a,1], Kai Xi[a], Shuqiang Jiao[b], R.I. Tomov[a,*], R. Vasant Kumar[a,*]

[a] Department of Materials Science and Metallurgy, University of Cambridge, Cambridge CB3 0FS, UK
[b] State Key Laboratory of Advanced Metallurgy University of Science and Technology Beijing, Beijing 100083, PR China

A B S T R A C T

LSCF/CGO composite cathodes decorated with small amount (less than 1 wt%) of nano CuO particles has been synthesized by infiltration technique. The area specific resistance (ASR) of the LSCF/CGO at 500 °C has been significantly reduced by the CuO infiltration from 15.5 Ω cm^2 and 0.62 Ω cm^2 to 3.9 Ω cm^2 and 0.32 Ω cm^2 at 500 °C and 650 °C respectively. The redox reaction of Cu^{2+}/Cu^{1+} at the interface of CuO and LSCF/CGO has been assigned as the main reason for the improvement. Lattice parameter change of LSCF at 500 °C has been detected by High Temperature XRD, indicating partial diffusion of Cu^{2+} into the lattice of LSCF, and formation of a new Cu containing compound. The performance stability of the infiltrated samples has been investigated by aging at 500 °C and 650 °C for 150 hours in stagnant air. A slight degradation of the catalytic property was observed during the aging process. The degradation may be attributed to three factors: (i) the coarsening of CuO nanoparticles, (ii) segregation of the SrO due the lattice change and (iii) instability of the new Cu^{2+} contained compounds.
© 2017 The Authors. Published by Elsevier Ltd. This is an open access article under the CC BY license (http://creativecommons.org/licenses/by/4.0/).

1. Introduction

Due to the fast-growing energy demand and the increasing urgency for environmental protection, clean energy sources have become an inevitable technological objective. However, until 2011, the world energy consumption based on the use of clean energy was only 9.8% according to the International Energy Agency (IEA). Replacing conventional energy sources by clean energy sources has proven to be expensive and can hardly bring economic effects to local communities in the short run, especially in some developing countries [1–3]. Solid Oxide Fuel Cells (SOFCs) have been widely studied for more than 50 years as promising route towards clean and efficient energy, [4–6]. However, the production and operational costs still remain major barriers to the SOFCs commercialization. As reported by The Joint Program of the Department of Energy's (DOE's) and Battelle Company [7] in 2014, the main cost of a SOFC stack is contributed by the metal components which currently utilize high quality specialized alloys in order to withstand the corrosion at high operational temperatures. Hence reducing the working temperature is desirable as it would allow replacement of expensive metal components or

ceramic interconnectors by cheaper stainless steel. However, any reduction of the operational temperature will also dramatically suppress the catalytic activity of the electrodes, thus significantly compromising the cell output power. Therefore, it is critically important to explore novel materials and architecture solutions preserving the high catalytic activity of the SOFCs electrodes at reduced working temperatures.

In the recent years some significant and promising research has been done on the implementation of LSCF cathodes modified with various metals. Precious metals like Pt, Pd or Ag have been proven in the past to have very good catalytic properties for oxygen reduction reaction (ORR). However, the high cost has prevented their wide scale commercialization in the SOFC. Thus the use of low-cost transitional metals in the synthesis of the cathodes like Cu modifying the B-site of the ABO_3 lattice have been an object of significant interest. Some promising results were reported while the difficulties have been usually assigned to the chemical interactions of Cu at high sintering temperatures [8,9]. An alternative strategy in achieving higher catalytic activity in porous SOFC electrodes is the infiltration of active materials into the electrode backbone structure thus extending the TPB of the ORR reaction area by nano-decorating the electrode scaffolding. In the case of the cathode, the material could be either an ionic conductor, such as $Ce_{0.9}Gd_{0.1}O_2$ (CGO) or $Zr_{0.9}Y_{0.1}O_2$ (YSZ) infiltrated onto the surface of an electronic conductors' backbone, such as $La_{0.6}Sr_{0.4}Co_{0.2}Fe_{0.8}O_3$ (LSCF), $La_{0.6}Sr_{0.4}MnO_3$ (LSM) and $Ba_{0.5}Sr_{0.5}Co_{0.8}Fe_{0.2}O_3$

* Corresponding authors.
  E-mail address: rvk10@cam.ac.uk (R.I. Tomov).
[1] Both authors contributed equally to this work.

(BSCF) or vice versa [10,11]. The combination of LSCF and CGO are commonly used as cathode materials for SOFC and the infiltration of LSCF onto CGO scaffold has been extensively studied and proved to be an effective way to reduce the operating temperature [12–14]. An alternative option is the infiltration of metal nitrate ink (e.g Cu nitrate) into the composite cathode (e.g LSCF/CGO) and sintering at relatively low temperatures ($\sim$500 °C) thus forming nano-decoration pattern onto the surface of the composite porous scaffolding simultaneously avoiding the adverse effects of high temperature sintering [15]. Many efforts have been made to design and produce SOFCs operating successfully at 500 °C [16–18]. It has been stated that in order to keep a reasonable fuel cell voltage output at lower temperature, the ASR of the electrodes should not exceed the value of 0.1 Ω cm^2 [19,20]. Recently, the research group from Michigan State University has reported reduction of the cathode's ASR to 0.1 Ω cm^2 at 540 °C by pre-infiltration method [21]. This suggested the possibility for further reduction of the temperature.

In this work, we attempted to enhance the catalytic efficiency of LSCF/CGO composite cathode operating at 500 °C by infiltrating small amount of CuO nanoparticles into a porous composite scaffolding. CuO/CeO$_2$ has been previously reported as good catalyst due to its synergistic redox and interaction property on the Cu-Ce interface [22–24]. The formation of CuO$_{1-\delta}$ nano percolation can produce oxygen vacancies and provide another pathway for the oxygen ions. In addition, if Cu$_2$O is not in thermodynamic equilibrium; it tends to chemisorb oxygen by donating electrons to form O^{2-} and CuO. The oxygen anions can hop into the vacancies of the nearby oxide ion conductors and allow the resulting Cu$^+$ ion to further chemisorb oxygen from the environment [25].

2. Experimental Section

Commercial La$_{0.6}$Sr$_{0.4}$Co$_{0.2}$Fe$_{0.8}$O$_3$ (d50: 0.10-0.50 μm, surface area: 10.0-14.0m^2/g, Fuel Cell Materials), denoted as LSCF, Ce$_{0.9}$Gd$_{0.1}$O$_2$ (d50: 0.10-0.50 μm, surface area: 10.0-14.0m^2/g, Sigma-Aldrich), denoted as CGO, and hydroxypropyl cellulose (M$_w$: 100,000, particle size: 20 mesh, Sigma-Aldrich) were used for inks preparation. To make CGO electrolyte, CGO with 5 wt% of hydroxypropyl cellulose were ball milled by zirconium dioxide balls with ethanol for 24 hrs at 300 rpm. The addition of ethanol helped to form floating phase during ball milling to dissolve the cellulose and enhance the milling efficiency. After milling, the mixture was dried at 90 °C for 10 hrs and grounded with mortar to break the agglomerated particles. Then, the powders were uniaxially pressed into discs with diameters of 1.3 cm at a 195 kg/cm^2 pressure by using stainless steel die. The resulting green CGO discs were heat treated at 400 °C for 1hr to burn off the binder and sintered at 1400 °C for 4 hrs. The heating and cooling rates were 5 °C/min.

Symmetrical cells were produced by inkjet printing of LSCF/CGO cathode composite ink on both sides of the fully dense CGO discs. The preparation of stable suspension inks is of critical importance for achieving repeatable jetting and avoiding clogging of the nozzles. The nozzle orifice diameter used in this work was 100 μm. In order to minimise the risk of clogging, care was taken to limit the powder particle size to below the empirically established level of 3 μm. The commercial LSCF and CGO powders were mixed with alpha-Terpineol and binders, and ball milled with 3YSZ beads in 3YSZ bowls in a planetary mill. Alpha-Terpineol acted as ink carrier as well as an efficient dispersant. The particle sizes of the as-prepared inks were analysed and a bimodal distribution was observed with a major peak centred at $\sim$0.2-0.4 μm diameter and a smaller broad tail towards larger diameters. The mass load of the inks was limited by the rheological working window of the nozzle, which defined the regime of stable repeatable jetting. Hence the
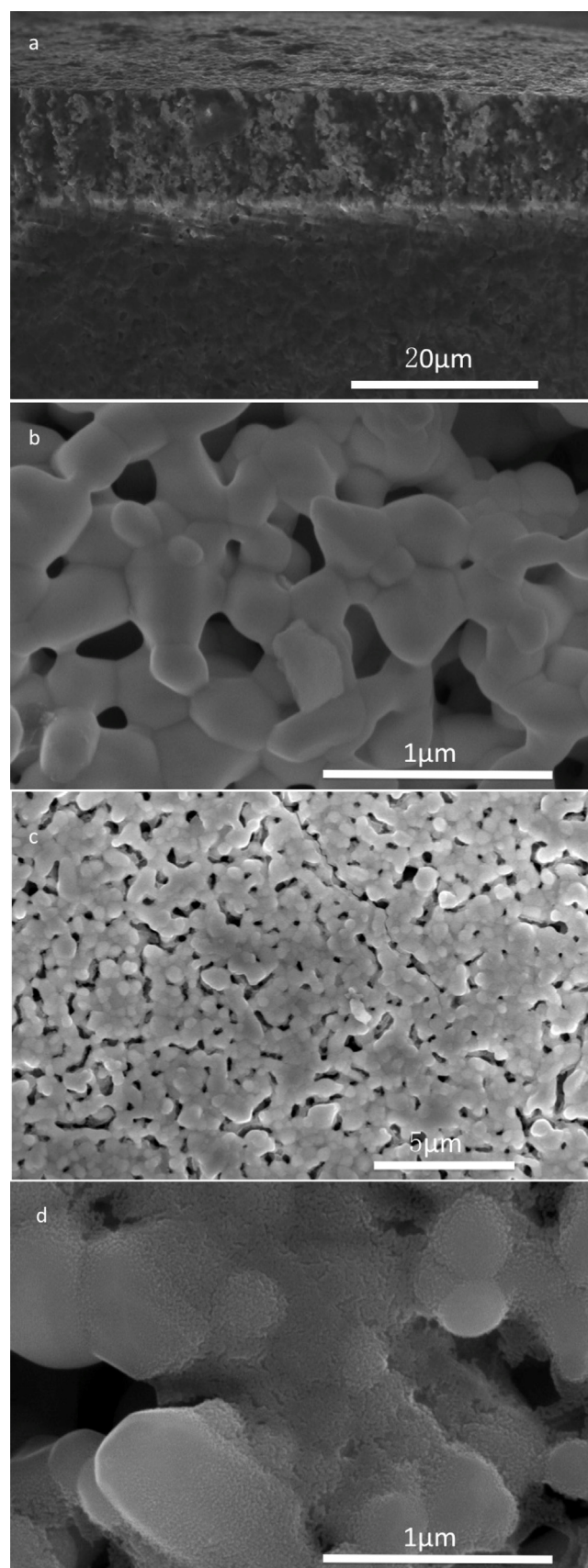

Fig. 1. Cross section of the LSCF/CGO cathode before CuO infiltration (a) and a microstructure of LSCF/CGO cathode's surface without infiltration (b). Microstructure of CuO infiltrated LSCF/CGO cathode's surface aged at 500 °C.

viscosity of the suspension inks had to be adjusted to suitable levels by adding another lower viscosity solvent. The suspension inks were sufficiently stable to permit printing without further mechanical agitation. The inks were additionally filtered through $3 \mu m$ glass microfiber filters before being loaded into an electromagnetic modified "Domino" inkjet nozzle compartment. The nozzle was used to produce symmetric cells with porous $10 \mu m$ thick cathode coatings. As-prepared cells were heated in air to $400 °C$ for 1hr to burn the polymer ink vehicle off and then heated to $1150 °C$ for 2 hrs to form the porous cathodes. Ramping rates of $5 °C/min$ of heating and cooling was used.

To produce CuO infiltrated cathodes, impregnation solutions of $1 M$ $Cu(NO_3)_2$ were prepared by dissolving $Cu(NO_3)_2$ $3H_2O$ (Sigma Aldrich) with appropriate amount of citric acid (mole ratio of Cu^{2+} to Citric acid is 1:1.5) into a mixture of distilled water and ethanol (volume ratio of 1:2). The ethanol was used to enhance the wettability of the ink due to its lower surface tension. The infiltration process was carried out by placing a drop of metal nitrate solution onto the surface of the cathode (sequentially on both sides). The solution was permeated into the cathode by capillary action under vacuum. After that, the pellets were heat treated at $500 °C$ in air for 30mins in order to decompose the metal nitrate and form metal oxide nanoparticles. Heating and cooling rates of $5 °C/min$ were employed. Finally, the symmetric cells were coated by silver mesh and the polarization curves were measured by impedance spectroscopy (Solarton SI 1287 electrochemical interface and SI 1260 impedance/gain-phase analyser, frequency range − $0.01Hz$–$100000 Hz$ and AC amplitude − $10 mV$). Phase transition and lattice parameter change of LSCF during heating from $50 °C$ to $750 °C$ (interval temperature − $50 °C$, heating rate − $3 °C/min$, measurement duration for each point − 15mins) has been examined by High temperature XRD (D8 advance Bruker powder diffractometer). Microstructure of the sample has been observed by FEI Nova NanoSEM FEG and the element distribution was measured by EDX mapping.

3. Results and discussion

The cross-section of a single symmetric cell before CuO infiltration with dense electrolyte and porous electrodes (10–$15 \mu m$ in thickness) obtained by the as-described sintering procedure is shown in Fig. 1a and b. Infiltration of CuO introduced dense and uniform nanoparticles decoration distributed on the cathode surface (see Fig. 1c and d). The average particle size $\sim 10 nm$ was estimated by high resolution SEM. Analysing the surface composition by EDX confirmed these nanoparticles as CuO.

EDX mapping showed the surface of LSCF/CGO cathode was fully covered by CuO nanoparticles (see Fig. 2). The amount of CuO on the surface detected by the EDX probe was approx. 5at%. These CuO particles has coarsened to $50 nm$ and $400 nm$ after aging at $500 °C$ and $650 °C$ respectively. The EIS Nyquist plots and the evolution of area-specific resistances (ASRs) vs time at $500 °C$ and $650 °C$ are shown in Fig. 3.

A significant reduction of ASR from $15.5 \Omega cm^2$ and $0.62 \Omega cm^2$ to $3.9 \Omega cm^2$ and $0.32 \Omega cm^2$ was observed at both $500 °C$ and $650 °C$ as a direct result of the infiltration (see Fig. 3a and b) while the Ohmic resistance of the cells did not seem to be affected by either infiltration or aging. After aging, the ASR of non-infiltrated sample at $500 °C$ and $650 °C$ has increased to $64.1 \Omega cm^2$ and $1.95 \Omega cm^2$ whereas that of the CuO infiltrated sample has only increased to $20.3 \Omega cm^2$ and $0.54 \Omega cm^2$ (the ASR was calculated as $ASR = (1/2S)*R$, S is the total surface area of the cathode, $0.78 cm^2$, and R is the total resistance contributed by the cathode on both side of the electrolyte, which is extracted from the distance between the two intersection points of the semicircle on the Nyquist plot with Z" axis as shown in Fig. 3a and b).
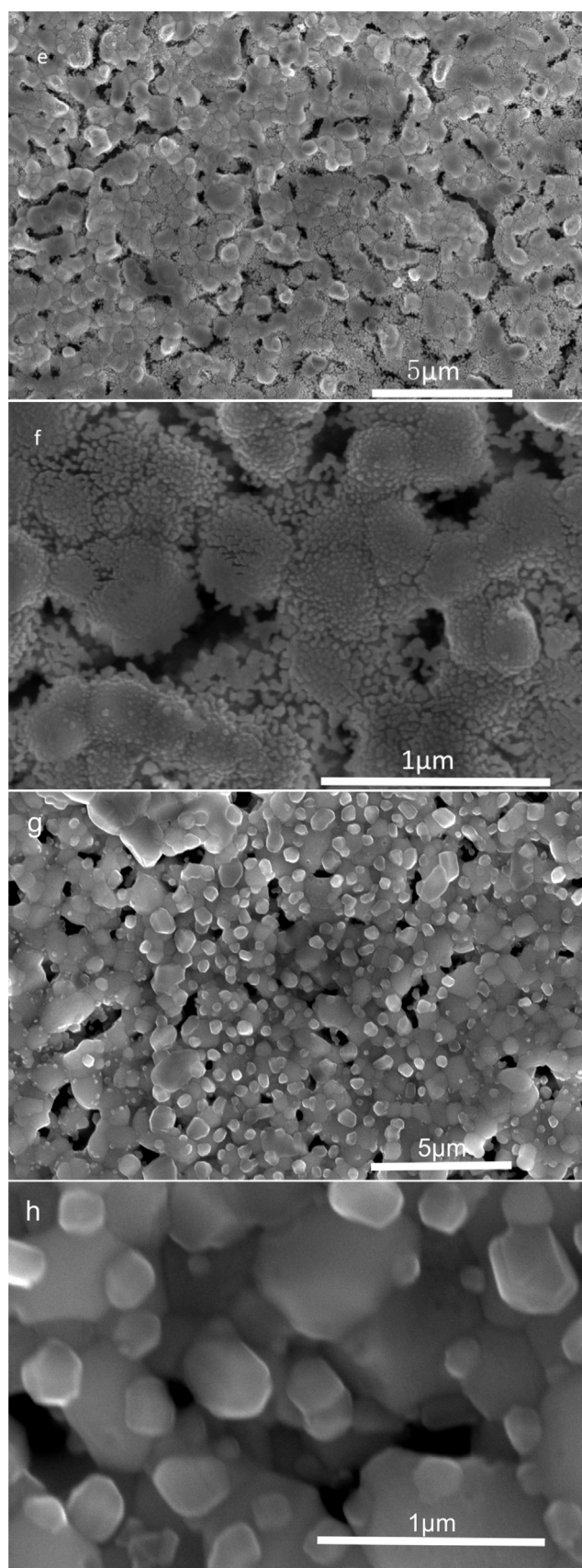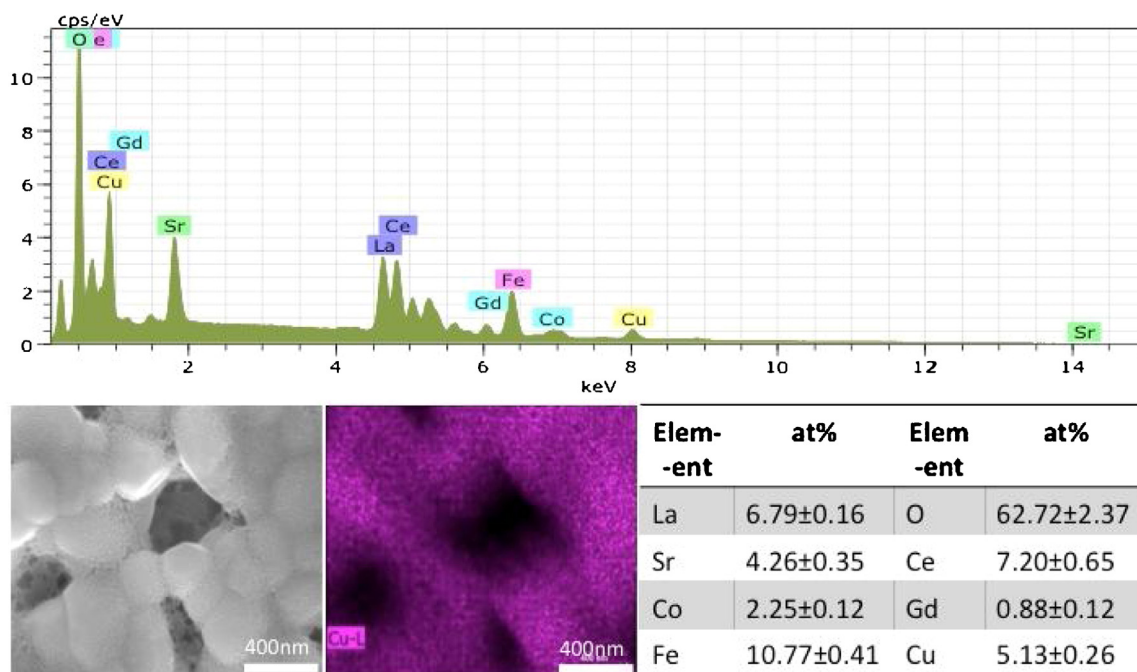

Fig. 1. (Continued)

Fig. 2. Distribution of CuO nanoparticles on the LSCF/CGO cathode's surface obtained by EDX mapping.

Both the degradation of LSCF/CGO and the catalytic enhancement due to the CuO infiltration was more significant at 500 °C. The observed ASR reduction suggested that the infiltration with CuO could reduce and stabilize the cathode working temperature in the temperature range of 500 °C–650 °C. Although the performance of CuO infiltrated sample also degraded, it gradually reached the steady state after 150 hours (see Fig. 3c and d). It could be speculated that the ASR of CuO infiltrated LSCF/CGO would remain at this stable level during the long-term operation. Therefore, CuO infiltration could be an efficient and cost-effective way to enhance
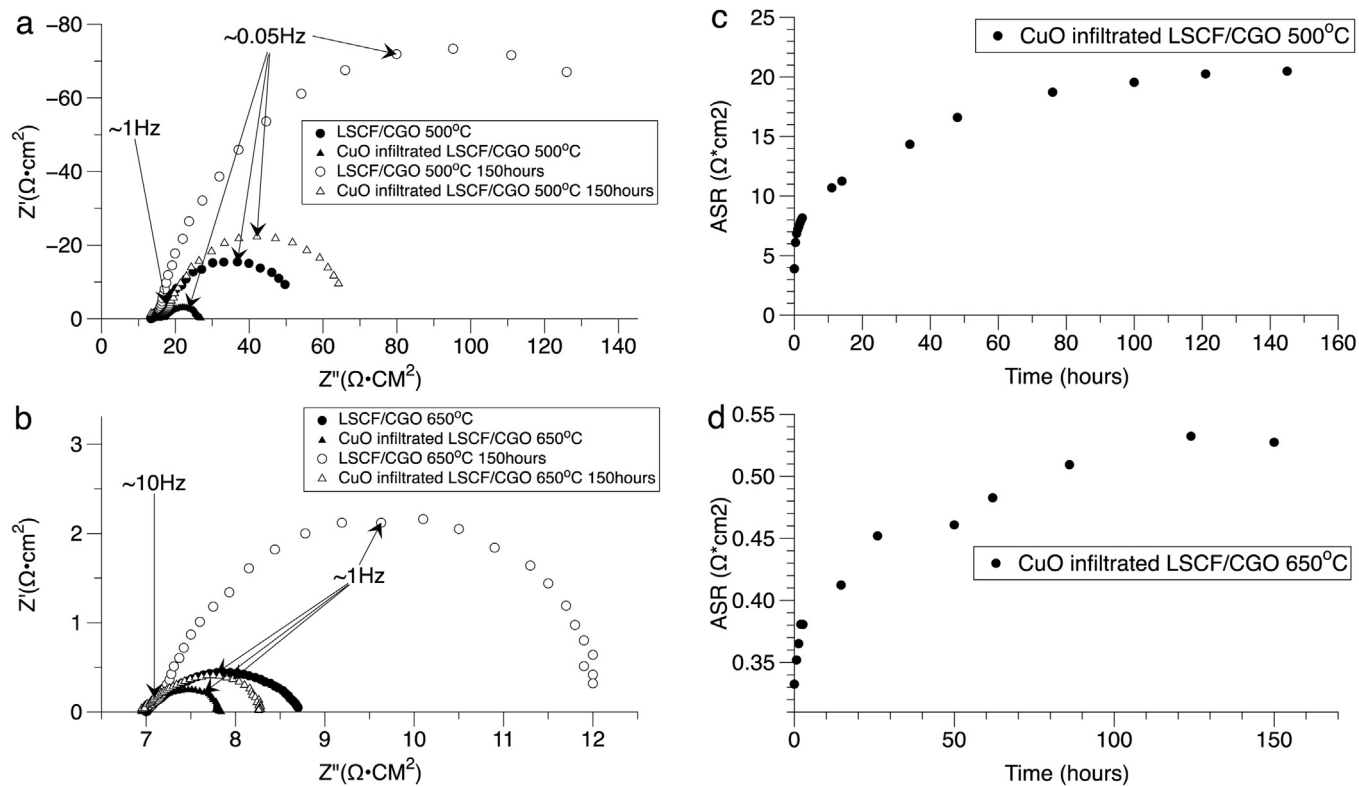

Fig. 3. Impedance spectra of symmetrical cells infiltrated with CuO plus a reference non-infiltrated sample measured before and after aging 150 hours at (a) 500 °C and (b) 650 °C; (b) (c) ASR of CuO infiltrated LSCF/CGO increased during aging at 500 °C and (d) at 650 °C.
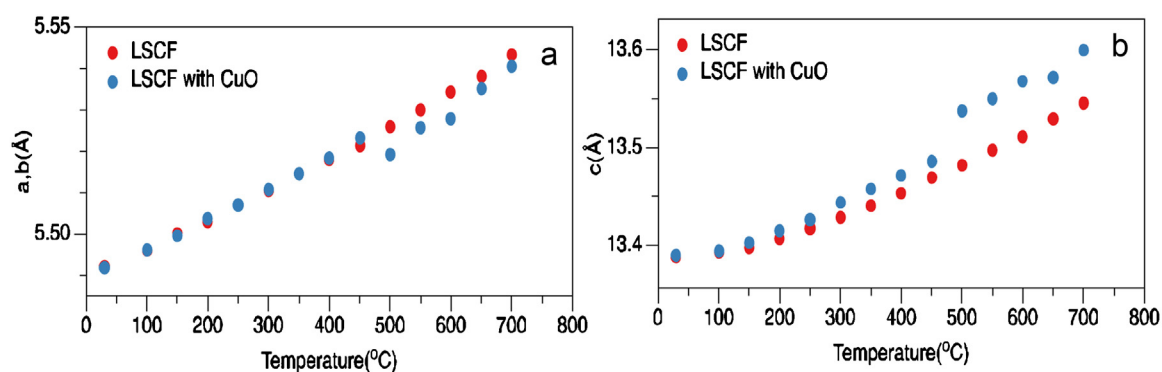
Fig. 4. Lattice parameter change of LSCF vs. temperature − (a) a and b axis and (b) c axis, with and without the infiltration of CuO.

the catalytic stability of LSCF/CGO cathode. In order to further optimize the infiltration procedure, we needed to understand the mechanism leading to the observed improvement of ORR reaction efficiency as well as enhanced operational stability. It was considered that in the as-described experimental conditions Cu could either stay on the surface of LSCF/CGO or diffuse into its lattice. Hence, the catalytic property of LSCF/CGO could be affected by two possible processes.

In the first scenario, ORR reaction would be affected at the interface between CuO and LSCF/CGO where CuO acted as catalyst. The oxidation state change of Cu^{2+}/Cu^{+} would create oxygen vacancy facilitating the catalytic process so that the ASR was effectively reduced. During aging, the small CuO particles

aggregated and coarsened, as shown in Fig. 1(d) and (f), due to their high mobility. Consequently, the length of the CuO-LSCF/CGO interface was reduced accordingly, leading to the reduction of the length of the contact boundary between CuO and LSCF/CGO.

Another possible process is the diffusion of Cu^{2+} into the LSCF lattice. We explored the LSCF cell parameters with high temperature XRD (step interval of 50 °C). The results indicated that the infiltration of CuO into the composite LSCF/CGO cathode led to a noticeable change in the lattice parameters of the cathode material at approximately 500 °C as shown in Fig. 4(a) and (b).

As clearly seen in Fig. 4, the unit cell of infiltrated LSCF was elongated along the c- axis and shrank inward along a- and b- axes at ∼450 °C–800 °C. We speculate that this nonlinear change
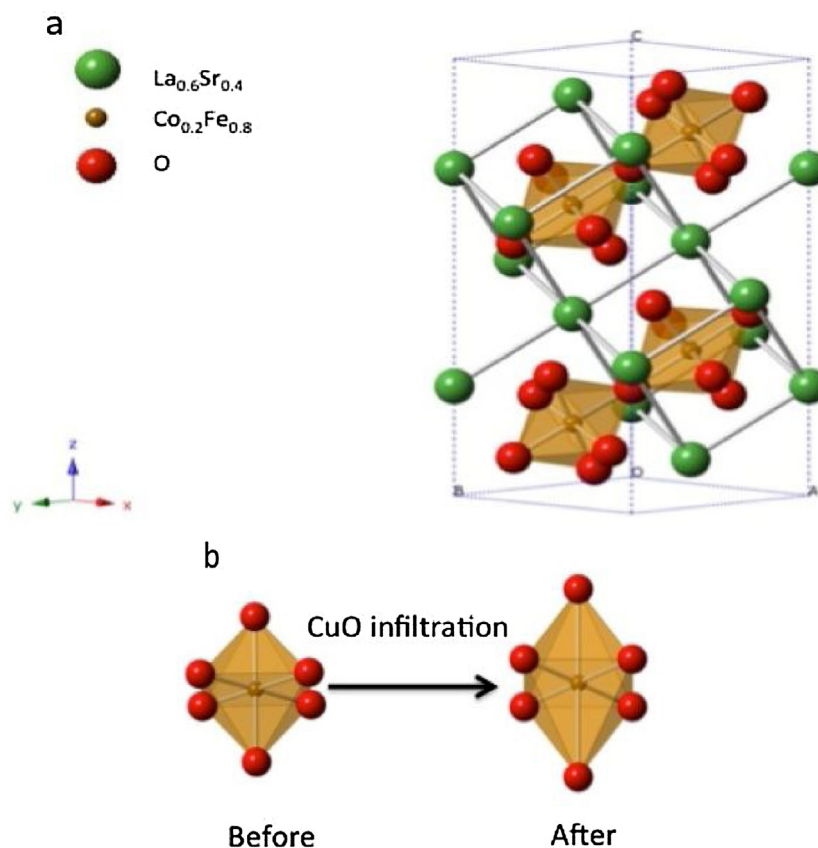

Fig. 5. (a) Unit cell model of LSCF and (b) The influence of the Jahn Teller's effect due to the formation of six-coordinate Cu complex after CuO infiltration (drawn by Crystal Maker).
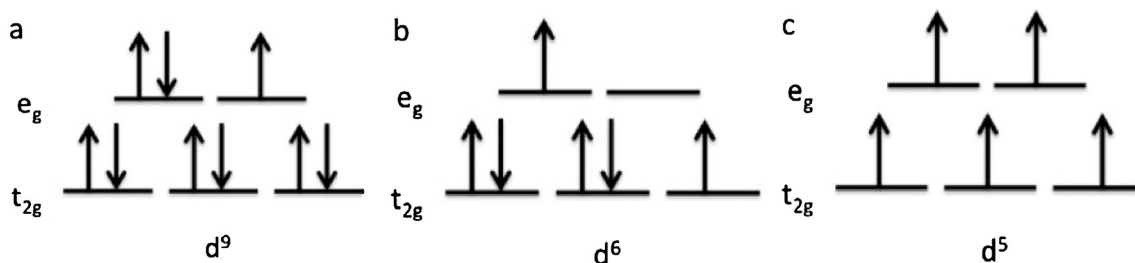
Fig. 6. The electronic configuration of (a) Cu^{2+}, (b) Co^{3+} and (c) Fe^{3+}.

(within 50 °C and 30mins)of the lattice parameter was quite likely caused by a phase transition rather than chemical expansion or thermal expansion.

LSCF is a perovskite with a rhombohedral structure as shown in Fig. 5(a) having space group R–3C H(167) (where the space group of a perovskite structure in a cubic system is pm3 m and the coordinates number of the atoms was set by referencing the ICSD database [26]).

Each unit cell contains 2 complete perovskite structures and 4 octahedrons. Each octahedron consists of 6 oxygen atoms on the corners and 1 $Co_{0.2}Fe_{0.8}$ in the middle as shown in Fig. 5(a). Cu^{2+} is not likely to be doped into the A (La, Sr)-site due to the ionic size mismatch but it is a candidate dopant on the B (Co, Fe)-site. Therefore, after the infiltration of CuO, at sufficiently high temperature Cu^{2+} can diffuse into the B site to substitute Co^{3+} or Fe^{3+} ions and to form six oxygen coordinate Cu^{2+} complex as shown in Fig. 5(b). Cu^{2+} has d^9 electronic configuration ($1s^2 2s^2 2p^6 3s^2 3p^6 d^9$) thus giving Cu^{2+} a degenerate ground state due to the two possible distributions of the electrons on the e_g orbit as shown in Fig. 6(a). Due to the degeneracy, the repulsion forces along x, y and z directions between Cu^{2+} and O^{2-} will change. To remove the degeneracy these octahedrons will be distorted (Jahn-Teller's distortion), and the distance between Cu^{2+} and O^{2-} will change. For Co^{3+} with d^6 electron configuration, which has an intermediate spin state ($t_{2g}^5 e_g^1$) [27], the degeneracy is on both high and low energy state (See Fig. 6(b)). However, there is only one electron on high-energy state (e_g) and the distortion from the low-energy state is relatively negligible (t_{2g}). The repulsion force will be much smaller than Cu^{2+}, which has three electrons on the high-energy state. The high spin Fe^{3+} has a d^5 electron configuration with no degeneracy ($t_{2g}^3 e_g^2$) [28]. Therefore, there is no expectation of Jahn Teller distortion due to Fe^{3+} (See Fig. 6(c)). Therefore, once Cu^{2+} goes into the LSCF's lattice, the lattice parameters are expected to change as evidenced by the observed XRD results.

Jahn Teller distortion in Cu^{2+}-contained composites has been extensively studied [29–32] and the lattice strain due to Cu^{2+} substitution has become a common example demonstrating the Jahn Teller effects. We assume that the lattice parameter change of LSCF after the CuO infiltration is a result of Cu substitution into the LSCF lattice. As a consequence, the infiltration of CuO can increase the instability of the lattice due to the lattice strain and cause enhanced segregation of SrO. The segregation of SrO is a commonly observed phenomenon in LSCF cathodes [33–36] and was found to
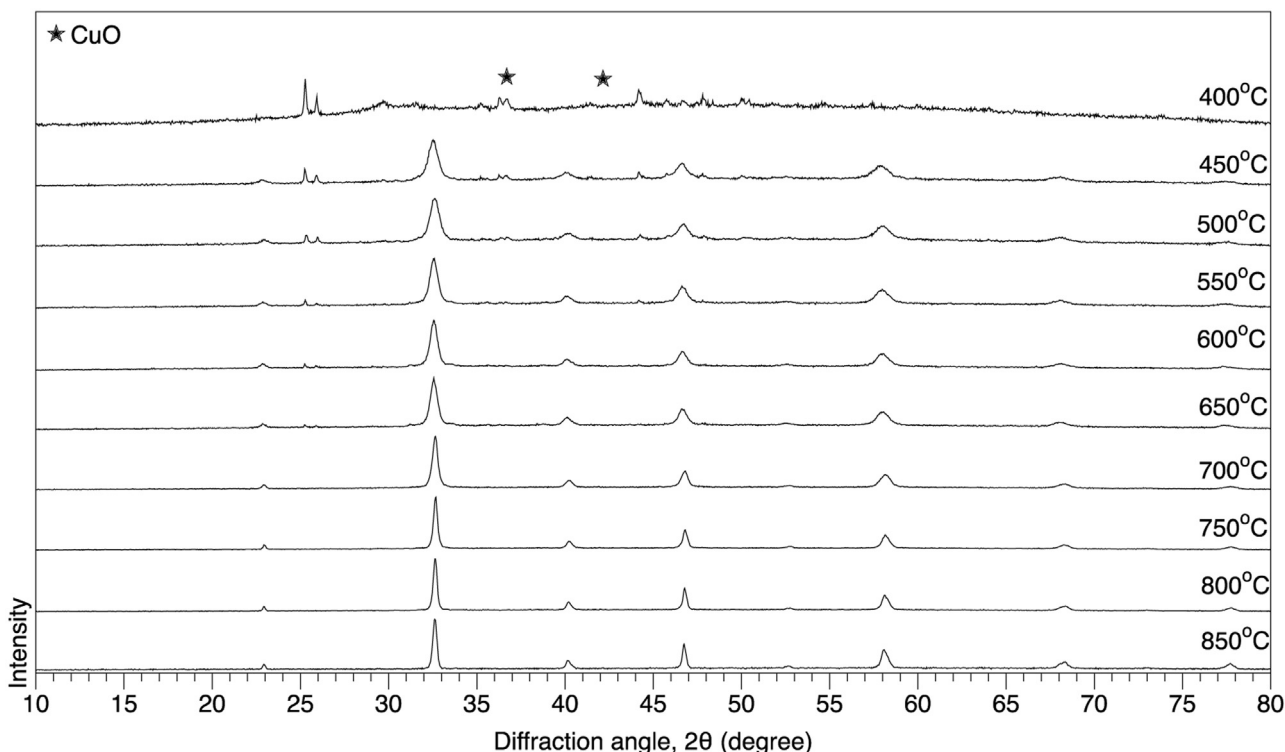

Fig. 7. XRD of "LSCuF" synthesized by different temperature.

be an inherent reason of the degradation of LSCF based cathodes. In addition, Co_2O_3 or Fe_2O_3 can also segregate to balance the internal charge. The resulting segregation of nanoparticles is expected to occur on the surface of the cathode backbone. As mentioned by [33], such segregation was occurring also in non-infiltrated LSCF cathodes taking place at the top surface or near surface region while the overall composition has not changed. The effect was linked to the high oxygen non-stoichiometry inherent to the LSCF.

Due to the limited resolution of the EDX, it was hard to distinguish between Cu, Co, Fe and Sr signals generated from the surface and bulk. However, as the effect of diffusion of CuO was observed we tried to verify evidence of the existence of a Cu containing compound by synthesis of a new cathode material replacing Co with Cu in order to obtain $La_{0.6}Sr_{0.4}Cu_{0.2}Fe_{0.8}$ (LSCuF). LSCuF powder has been synthesized via sol gel method. Stoichiometric amount of La, Sr, Cu and Fe nitrate was mixed with citric acid (metal ion(mole): citric acid(mole) = 1:1.5) in water. The as prepared solution was dried at 80 °C for the sol-gel process and calcined at different temperatures from 400 °C to 800 °C and cooled to room temperature. Room temperature XRD (Bruker D8) tests of the as–synthesized powder was performed exploring phase dynamic of the new perovskite structure at different calcination temperatures as shown in Fig. 7.

Bellow 450 °C, the powder mixture was still a composite of poly-crystalline and nano-crystalline powders while the perovskite structure formation started above 450 °C. A single phase LSCuF was obtained when the calcination temperature reached levels above 700 °C. The peaks of CuO are indicated in Fig. 7 by star signs (referencing the PDF 78-0428-ICSD database). The XRD results confirmed that CuO was incorporated into the solid solution at approximately 500 °C. Therefore, the formation of partially substituted LS(Co)CuF at 500 °C in the CuO infiltrated LSCF/CGO cathode was considered plausible.

The impedance spectroscopy of identical LSCF/CGO and LSCuF/CGO (1:1) symmetrical cells has been tested at 500 °C in stagnant

air. The ASR of LSCuF/CGO was measured to be approximately 10 Ω cm^2, which was significantly lower than the value measured for the LSCF/CGO composite cathode as shown in Fig. 8(a). The degradation of LSCuF based cell after 10 h at 500 °C (see Fig. 8(b)) was observed to have similar trend to that of Cu infiltrated LSCF/CGO cell as presented on Fig. 3(b).

These two results indicated that the improvement of catalytic property of LSCF/CGO cathode due to the infiltration of CuO could be attributed not only to the promotion of the redox reaction taking place at the CuO-LSCF/CGO interface but also to the formation of new bulk compound as per formation of LS(Co)CuF or other Cu contained compound. Following the same logic, the performance degradation could be caused not only by the coarsening of the CuO nanoparticles but also due to the instability of LSCuF.

4. Conclusions

The infiltration of a composite LSCF/CGO cathode with Cu nitrate inks and the consequent formation of CuO nano-decoration was proven to successfully reduce the polarization resistance of the cathode in both short and long term. The effect was more pronounced at low working temperature (500 °C) but deteriorated to some extent after 150 h aging in stagnant air.

The improvement of the cathode catalytic property by CuO infiltration before aging may be due to two reasons:

1. The oxidation state change of the Cu^{2+}/Cu^{1+} on the cathode's surface creating oxygen vacancies near the CuO-LSCF/CGO interface and accelerating the incorporation of oxygen from the environment.
2. The diffusion of Cu^{2+} into the LSCF lattice, forming new Cu containing compounds, such as LSCoCuFe, and thus facilitating an improvement of the overall activation polarization losses.

The observed better long term stability of the infiltrated vs the non-infiltrated symmetrical cells suggested that Cu substitution in the LSCF lattice maybe responsible for an inhibition of SrO nanoparticles segregation on the LSCF surface responsible for suppressing the catalytic activity on the surface of the scaffold. The degradation of the infiltrated cathode observed after aging at 500 °C for 150 hours could be attributed to three factors:

1. The observed coarsening of the Nano CuO particles after 150 hours which significantly reduced the length of the CuO-LSCF/CGO interface.
2. CuO interaction with LSCF, resulting in the internal strain of the LSCF lattice.
3. The new Cu containing compound could be unstable during long-term exposure to 500 °C.

Fig. 8. (a) ASR of LSCF, CuO infiltrated LSCF and LSCuF before aging (b) the degradation of LSCuF after 10 hours.

Notes and references

[1] I.K. Maji, Does clean energy contribute to economic growth? Evidence from Nigeria, Energy Reports 1 (2015) 145–150.
[2] W. Xie, P. Sheng, X. Guo, Coal, oil, or clean energy: Which contributes most to the low energy efficiency in China? Util. Policy 35 (2015) 67–71.
[3] H.-T. Pao, Y.-Y. Li, Hsin-Chia Fu, Clean energy, non-clean energy, and economic growth in the MIST countries, Energy Policy 67 (2014) 932–942.
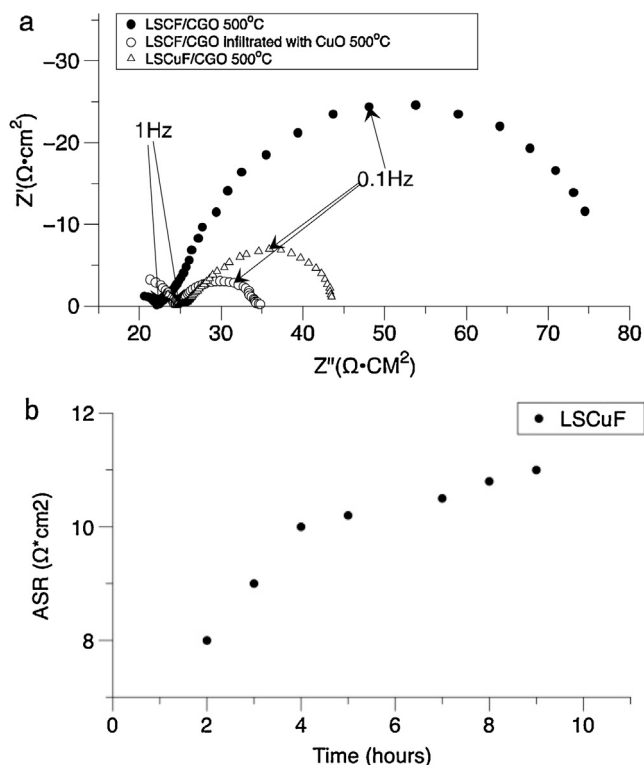
[4] M.L. Perry, T.F. Fuller, A historical perspective of fuel cell technology in the 20th century, J. Electrochem. Soc. 149 (7) (2002) S59–S67.

[5] H. Möbius, On the history of solid electrolyte fuel cells, J. solid state Electrochem. (1997) 2–16.

[6] J.M. Andújar, F. Segura, Fuel cells: History and updating. A walk along two centuries, Renew. Sustain. Energy Rev. 13 (December (9)) (2009) 2309–2322.

[7] A. Pplications, Manufacturing Cost Analysis of 1 Kw and 5 Kw Solid Oxide Fuel Cell (Sofc) for Auxilliary Power Applications, (2014) .

[8] L.F.L. Shaoli Guo, Hongjing Wu, Fabrizio Puleo, B-Site Metal (Pd, Pt, Ag, Cu, Zn, Ni) Promoted La 1-xSrxCo 1-yFeyO3-δ Perovskite Oxides as Cathodes for IT-SOFC, catalysts (2015) 366–391.

[9] C.V.A.C. Haanappel, B. Bär, C. Tropartz, J. Mertens, F. Tietz, Various Lanthanum Ferrite-Based Cathode Materials With Ni and Cu Substitution for Anode-Supported Solid Oxide Fuel Cells, J. Fuel Cell Sci 7 (December) (2015) 1–4.

[10] S. Jiang, W. Wang, Novel structured mixed ionic and electronic conducting cathodes of solid oxide fuel cells, Solid State Ionics 176 (15–16) (2005) 1351–1357.

[11] X. Ding, W. Zhu, X. Gao, G. Hua, J. Li, Nanoparticles for Intermediate Temperature Solid Oxide Fuel Cells, Fuel Process. Technol. 135 (2014) 6–11.

[12] M. Shah, S. Barnett, Solid oxide fuel cell cathodes by infiltration of La0.6Sr0.4Co0.2Fe0.8O3-δ into Gd-Doped Ceria, Solid State Ionics 179 (35–36) (2008) 2059–2064.

[13] Y. Liu, F. Wang, B. Chi, J. Pu, L. Jian, S.P. Jiang, A stability study of impregnated LSCF-GDC composite cathodes of solid oxide fuel cells, J. Alloys Compd. 578 (2013) 37–43.

[14] M. Shah, P.W. Voorhees, S.A. Barnett, Time-dependent performance changes in LSCF-infiltrated SOFC cathodes: The role of nano-particle coarsening, Solid State Ionics 187 (1) (2011) 64–67.

[15] Z. Liu, B. Liu, D. Ding, M. Liu, F. Chen, C. Xia, Fabrication and modification of solid oxide fuel cell anodes via wet impregnation/infiltration technique, J. Power Sources 237 (2013) 243–259.

[16] R. Doshi, Development of Solid-Oxide Fuel Cells That Operate at 500 °C, J. Electrochem. Soc. 146 (4) (1999) 1273.

[17] J. Huang, Z. Mao, Z. Liu, C. Wang, Development of novel low-temperature SOFCs with co-ionic conducting SDC-carbonate composite electrolytes, Electrochem. commun. 9 (10) (2007) 2601–2605.

[18] Y. Higuchi, M. Sugawara, K. Onishi, M. Sakamoto, S. Nakayama, Oxide ionic conductivities of apatite-type lanthanum silicates and germanates and their possibilities as an electrolyte of lower temperature operating SOFC, Ceram. Int. 36 (3) (2010) 955–959.

[19] D.M. Bastidas, High temperature corrosion of metallic interconnects in solid oxide fuel cells *, Revista De Metalurgia 42 (6) (2006) 425–443.

[20] M.D. Gross, J.M. Vohs, A Strategy for Achieving High-performance with SOFC Ceramic Anodes, Revista de Metalurgia 10 (4) (2007).

[21] T.E. Burye, J.D. Nicholas, Nano-ceria pre-infiltration improves La0.6Sr0.4Co0.8Fe0.2O3 infiltrated Solid Oxide Fuel Cell cathode performance Theodore, J. Power Sources 276 (2015) 54–61.

[22] X. Tang, B. Zhang, Y. Li, Y. Xu, Q. Xin, W. Shen, CuO/CeO2 catalysts: Redox features and catalytic behaviors, Appl. Catal. A Gen. 288 (1-2) (2005) 116–125.

[23] X. Tang, B. Zhang, Y. Li, Y. Xu, Q. Xin, W. Shen, Carbon monoxide oxidation over CuO/CeO2 catalysts, Catal. Today 95 (2004) 191–198.

[24] C. Xu, X. Hao, M. Gao, H. Su, S. Zeng, Important properties associated with catalytic performance over three-dimensionally ordered macroporous CeO2-CuO catalysts, Catal. Commun. 73 (2016) 113–117.

[25] W. Dow, T. Huang, Yttria-Stabilized Zirconia Supported Copper Oxide Catalyst, J. Catal. 182 (136) (1996) 171–182.

[26] X. Chen, S.P. Jiang, Highly active and stable (La0.24Sr0.16Ba0.6) (Co0.5Fe0.44Nb0.06)O3-d (LSBCFN) cathodes for solid oxide fuel cells prepared by a novel mixing synthesis method, J. Mater. Chem. A 1 (2013) 4871–4878.

[27] D. Louca, J.L. Sarrao, Dynamical disorder of spin-induced Jahn-Teller orbitals with the insulator-metal transition in cobaltites, Phys. Rev. Lett. 91 (15) (2003) 155501.

[28] K. Hui, L. Jie, Z. Changfei, Ultrasonic signature of Jahn-Teller effect in La1/3Sr2/3Co1-xFexO3 perovskites, Phys. B Condens. Matter 11 (2009) 1128–1131.

[29] J. Echeverría, E. Cremades, A.J. Amoroso, S. Alvarez, Jahn-Teller distortions of six-coordinate CuII compounds: cis or trans? Chem. Commun. (Camb) (28) (2009) 4242–4244.

[30] J.S. Zhou, J.A. Alonso, J.T. Han, M.T. Fernández-Díaz, J.G. Cheng, J.B. Goodenough, Jahn-Teller distortion in perovskite KCuF3 under high pressure, J. Fluor. Chem. 132 (12) (2011) 1117–1121.

[31] M. Zlatar, M. Gruden-Pavlović, C.W. Schläpfer, C. Daul, Intrinsic Distortion Path in the analysis of the Jahn-Teller effect, J. Mol. Struct. THEOCHEM 3 (2010) 86–93.

[32] T. Onishi, K. Yamaguchi, Theoretical calculations of effective exchange integrals by spin projected and unprojected broken-symmetry methods II: Cluster models of Jahn-Teller distorted K2CuF4 solid, Polyhedron 10 (2009) 1972–1976.

[33] H. Ding, A. Virkar, M. Liu, F. Liu, Suppression of Sr surface segregation in La1-xSrxCo1-yFeyO3-δ: A First Principles Study, Phys. Chem. Chem. Phys. (2012) 489–496.

[34] B. Wei, K. Chen, L. Zhao, Z. Lü, S. Ping Jiang, Chromium deposition and poisoning at La0.6Sr0.4Co0.2Fe0.8O3-d oxygen electrodes of solid oxide electrolysis cells, Phys. Chem. Chem. Phys. 17 (3) (2015) 1601–1609.

[35] M. Finsterbusch, A. Lussier, J.A. Schaefer, Y.U. Idzerda, Electrochemically driven cation segregation in the mixed conductor La0.6Sr0.4Co0.2Fe0.8O3-δ, Solid State Ionics 212 (2012) 77–80.

[36] W. Araki, T. Yamaguchi, Y. Arai, J. Malzbender, Strontium surface segregation in La0.58Sr0.4Co0.2Fe0.8O3-δ annealed under compression, Solid State Ionics 268 (2014) 1–6.